Journal of The Electrochemical Society, **154** (9) A875-A881 (2007)
0013-4651/2007/154(9)/A875/7/$20.00 © The Electrochemical Society

Effects of Iron Addition on Material Characteristics and Pseudo-Capacitive Behavior of Mn-Oxide Electrodes

Ming-Tsung Lee, Jeng-Kuei Chang,*,z and Wen-Ta Tsai*

Department of Materials Science and Engineering, National Cheng Kung University, Tainan, Taiwan

Iron addition was attempted in this study to improve the pseudo-capacitive property of Mn oxides. The oxides were prepared on graphite substrates by anodic deposition. The deposition solutions were 0.25 M manganese acetate [$Mn(CH_3COO)_2$] aqueous solutions with various amount of $FeCl_3$ (up to 0.15 M). Crystal structure and surface morphology of the deposited oxides were examined by X-ray diffraction and scanning electron microscopy, while their chemical state was analyzed by X-ray photoelectron spectroscopy and X-ray absorption near edge structure. Moreover, specific capacitances of the oxide electrodes were determined by cyclic voltammetry in 2 M KCl electrolyte. Experimental results indicated that the incorporated iron presented as divalent and trivalent forms in the binary oxides. Although iron addition did not change the nanocrystalline structure of the deposited Mn oxide, it caused the chemical state and surface morphology variations of the oxide electrodes. Consequently, their pseudo-capacitive performances were modified. The optimum specific capacitance of 212 F g^{-1} was found for the oxide deposited in the solution containing 0.05 M $FeCl_3$. The value was 21% higher than that of the plain Mn oxide. Capacitance-retained ratio of the oxide after 1000 charge-discharge cycles was also improved from 70 to 85% because of iron addition.
 [DOI: 10.1149/1.2755880]

Manuscript submitted January 2, 2007; revised manuscript received May 15, 2007. Available electronically July 23, 2007.

Electrochemical capacitors (or supercapacitors) are charge-storage devices that have greater power density and longer cycle life than batteries, and they possess higher energy density as compared with conventional capacitors.[1] They have recently been considered to be a promising device in many fields, e.g., hybrid power sources, peak-power sources, backup-power storage, lightweight electronic fuses, starting power of fuel cells, etc.[2-4] Based on different energy-storage mechanisms, there are two kinds of electrochemical capacitors. Electric double-layer capacitors (EDLCs) and pseudo-capacitors have been examined. The former typically consists of electrodes (made of, for example, active carbon) with very high surface areas. The nonfaradaic separation of charges at the interface between a solid electrode and an electrolyte governs the capacitance of such a device.[5-7] The pseudo-capacitance arises from fast, reversible, and faradaic redox reactions that occur within bulk material of the electrode over an appropriate range of potentials.[2,8-10] Capacitance per unit area of the electrode material for psuedo-capacitors could be 10–100 times greater than that for EDLCs. In particular, amorphous hydrous ruthenium oxide has been demonstrated to exhibit excellent pseudo-capacitive performance (>700 F g^{-1}).[8] However, the high cost of ruthenium has limited its commercial use. Therefore, the search for a cheaper oxide with equivalent characteristics is attracting attention.

The natural abundance and low cost of Mn oxide, accompanied by its satisfactory electrochemical performance and environmental compatibility, have made it the most promising new electrode material for pseudo-capacitors. Recently, several researchers have begun to develop effective processes for producing Mn-oxide electrodes. The methods include thermal decomposition,[11] coprecipitation,[12] sol-gel process,[13-15] and anodic deposition.[16,17] Our previous studies[18-20] also showed that the Mn oxide deposited in manganese acetate aqueous solution had high specific capacitance, high power capability, and long cycle life. Though it was not extensively studied, iron oxide was another cost-effective alternative which could exhibit demanding pseudo-capacitive performance.[21-24] Wang et al.[23,24] reported that the magnetite (Fe_3O_4) electrode demonstrated an ideal capacitive behavior and possessed a specific capacitance as high as 170 F g^{-1} in the sodium sulfite electrolyte.

It is possible to manufacture a Mn/Fe binary oxide electrode that could present unique pseudo-capacitive performance which combines the advantages from both of the single-component oxide. Because literature concerning the preparation and property of this binary oxide electrode was rarely reported, Fe addition in the Mn oxide was attempted in this investigation by a simple anodic deposition process. The corresponding material and electrochemical characteristics were examined systematically. Fe/Mn content ratio within the oxides was controlled by adjusting the $FeCl_3$ concentration in the manganese acetate deposition solution. The deposited oxides were characterized by X-ray diffraction (XRD), scanning electron microscopy (SEM), X-ray photoelectron spectroscopy (XPS), and X-ray absorption spectroscopy (XAS). The pseudo-capacitive behavior of the oxide electrodes were also evaluated by cyclic voltammetry (CV).

Experimental

Mn/Fe oxides were electroplated onto 1×1 cm graphite substrates by anodic deposition at 25°C. The substrates were first polished with SiC paper of 800 grit, degreased with acetone and water, then etched in 0.2 M H_2SO_4 at 25°C, and finally washed with pure water in an ultrasonic bath. The plating solutions were 0.25 M manganese acetate aqueous solutions with various amounts of $FeCl_3$ addition (up to 0.15 M). During the deposition, the graphite substrate was maintained as the anode and a platinum sheet was used as the counter electrode. In addition, a saturated calomel electrode (SCE) was used as the reference electrode. An EG&G Princeton Applied Research model 263 potentiostat was employed to control the deposition conditions. Anodic deposition was performed under constant potential mode. The applied potential was 0.8 V (vs SCE) to give a total passed charge of 1.5 coulombs. After electrodeposition, the electrode was dried in air. The weight changes of the graphite substrates before and after deposition were measured using a microbalance with an accuracy of 1×10^{-5} g. The amount of loading oxides was found to be around 1.0–1.1 mg. The deposition process was found to be reproducible. The deposition time and weight of the oxides, prepared in the same solution, varied less than 5% from each other.

In order to explore the chemical composition of the deposited oxides, they were totally dissolved in a concentrated HCl aqueous solution and then evaluated by an inductively-coupled plasma (ICP) mass spectrometer (Hewlett Packard 4500). Crystal structure of the oxides with various amounts of Fe addition was determined by XRD. The patterns were recorded on a Rigaku D/MAX 2500 diffractometer with a glancing incident angle of 2°. The Kα radiation of copper target with a wavelength of 1.5418 Å was used as the X-ray source. The detected diffraction angle (2θ) was scanned from 20 to 80° with a speed of 1°/min. The surface morphology and chemical composition of the deposited oxides were examined with a scanning electron microscope (Philip XL-40FEG) and its auxiliary X-ray energy dispersive spectroscope (EDS). To quantitatively evaluate morphology of the oxide electrodes, the average surface

* Electrochemical Society Active Member.
z E-mail: catalyst@mail.mse.ncku.edu.tw

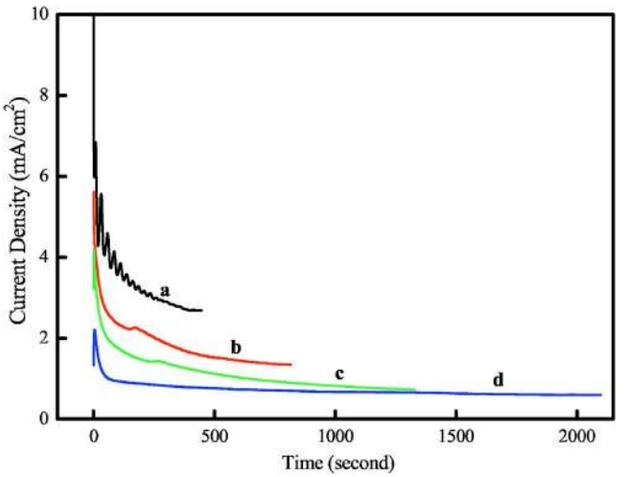

Figure 1. (Color online) Variations of anodic current density vs time during the various deposition processes. Curves a–d present the oxides deposited in the 0.25 M manganese acetate solutions with 0, 0.05, 0.10, and 0.15 M $FeCl_3$ addition, respectively.

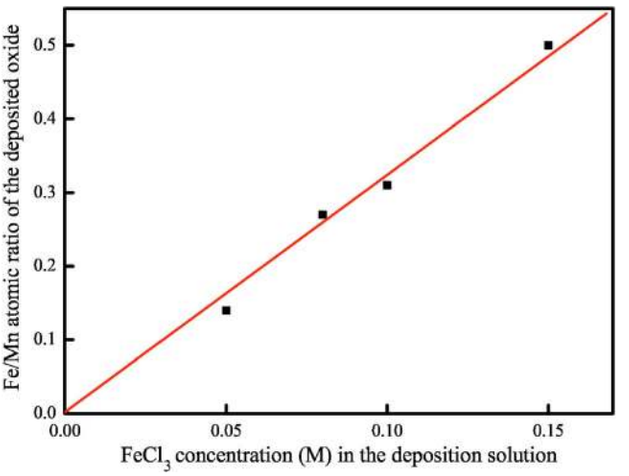

Figure 2. (Color online) Relationship between the Fe/Mn atomic ratio of the deposited oxide and the $FeCl_3$ concentration (M) in the deposition solution.

roughness (R_a) was measured with a confocal microscope (CM, Leica TCS SL). R_a is defined as integral of both the peak and valley area of the roughness profile divided by the evaluation length. The total area of the peaks above the mean line should be equal to the total area of the valleys below the mean line. XPS and XAS were also carried out to examine the chemical states of different oxides. XPS measurements were performed with an ESCA 210 (VG Science Ltd.) spectrometer. Monochromated Al Kα (1486.6 eV) radiation was utilized as the X-ray source. The pressure in the analyzing chamber was approximately 1×10^{-9} Torr during the measurements. Charge-up effect on the peak positions were corrected by reference to the C 1s signal of adventitious contamination hydrocarbon to 284.6 eV. The Fe $2p_{3/2}$ spectrum consisted of three components was represented by a Gaussian function on a Shirley-type background. XAS measurements were performed at the Taiwan Synchrotron Radiation Research Center (SRRC) using the Wiggler C beamline. Pure compounds of Mn_2O_3, MnO_2, FeO, and Fe_2O_3 were used as standard references in XAS analyses. The absorption threshold energy (E_0), which is known to be a critical factor for determining the valent state of the analyzed element, was obtained from the first inflection point in the main absorption range of the spectrum.

The pseudo-capacitive performance of the prepared oxides was characterized by CV in 50 mL 2 M KCl solution at 25°C. The test cell was a three-electrode system in which the oxide electrode was assembled as the working electrode. A platinum sheet and a SCE were used as the counter electrode and the reference electrode, respectively. The measuring instrument was also an EG&G 263 potentiostat. The potential was cycled within a potential range of 0–1 V (vs SCE) up to 1000 times. The CV scan rate was 25 mV s^{-1}. For specific capacitance evaluation, more than five samples were tested and the data shown in this study were the averages. The capacitance deviation between each sample was within 5%. In addition, the testing electrolyte (2 M KCl) was sampled and analyzed by an atomic absorption spectroscope (AAS, SOLAAR M6). The concentration of dissolved Mn and Fe from the oxides after CV cycling was thus examined.

Results and Discussion

Anodic deposition of Mn/Fe oxides.— Figure 1 shows the variations of current densities vs time during the deposition processes, which were performed in the 0.25 M manganese acetate solution with $FeCl_3$ addition up to 0.15 M. The results clearly indicated that the deposition rate decreased with increasing $FeCl_3$ concentration. For a total anodic pass charge of 1.5 C, the times required to deposit the oxides were 446, 815, 1328, and 2098 s, respectively, as 0, 0.05, 0.10, and 0.15 M $FeCl_3$ was added. During the oxide deposition process, the anodic reaction was as follows

$$Mn^{2+} + xH_2O \rightarrow MnO_x + 2xH^+ + (2x - 2)e^- \quad [1]$$

because the pH value of the plating solution decreased from 7 to 4 due to $FeCl_3$ addition, it may cause the retardation of the oxide deposition. An oscillation of the anodic current occurred during the deposition of the plain Mn oxide (as can be seen in curve a of this figure). It may be attributed to the exhaustion and resupply of the reactants near the electrode surface. However, as the deposition rate was decreased (as curves b–d), the current fluctuation could not be found anymore.

Fe/Mn content ratios of various deposited oxides were examined by ICP spectrometer and shown in Fig. 2. Analytic results confirmed that Fe was indeed incorporated into the Mn oxides. Moreover, the Fe/Mn atomic ratio was found to be linearly proportional to the $FeCl_3$ concentration in the deposition solution.

Crystal structure and surface morphology.— Figure 3 shows the XRD patterns of the oxide electrodes prepared in various deposition solutions. A pattern of the graphite substrate is also shown in this figure for comparison. Four patterns of the oxides with different Mn/Fe content ratios did not have visible differences. All the strong diffraction peaks were associated with the graphite substrates and were indexed with the corresponding diffraction planes in the figure. In each pattern, only a weak and broad peak located at the identical position of 37° was recognized. The peak was attributed to the deposited Mn oxide. It was also found that the diffraction intensity of this peak decreased with increasing the Fe addition amount. The results suggested that the incorporated Fe oxide could be amorphous and did not change the nanocrystalline structure of deposited Mn oxide.

Surface morphologies of various Mn/Fe oxides were examined by SEM and the micrographs are demonstrated in Fig. 4. The photos clearly illustrated that the Fe addition significantly affected the appearance of the oxide electrodes. For the plain Mn-oxide electrode, as shown in Fig. 4a, granular surface morphology was observed. As the $FeCl_3$ concentration in the plating solution continuously raised to 0.05 M, surface roughness of the deposited oxides gradually increased (as Fig. 4b and c). Many salients, due to Fe addition, were seen to stand on the surface of the electrodes and made the oxides rather rough. However, as can be confirmed in Fig. 4d, the surface roughness began to decrease as the $FeCl_3$ addition in the plating solution was further increased. Figures 4e and f show the morpholo-

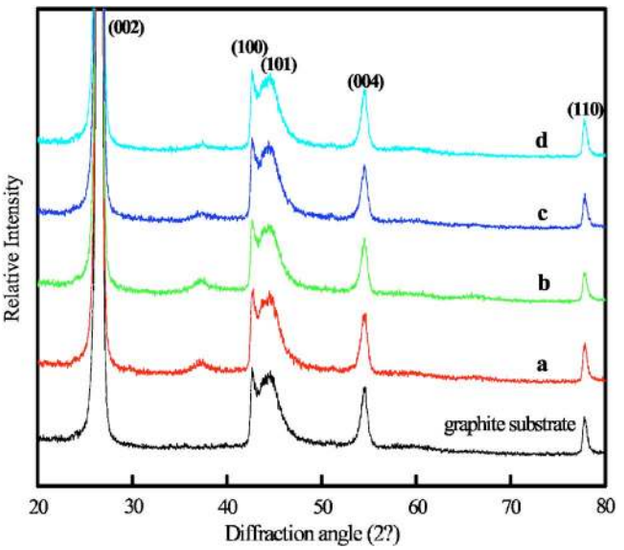

Figure 3. (Color online) XRD patterns of the various oxide electrodes. Curves a–d present the oxides deposited in the 0.25 M manganese acetate solutions with 0, 0.05, 0.10, and 0.15 M $FeCl_3$ addition, respectively. A pattern collected from the graphite substrate is also included.

gies of the oxides with much higher Fe addition (added $FeCl_3$ was 0.08 and 0.15 M, respectively). The surface became flat and was even smoother than the plain Mn oxide. Cracks observed on the surfaces of all the deposited oxides were probably caused by shrinkage stress during drying. Figure 5 shows EDS mapping results of

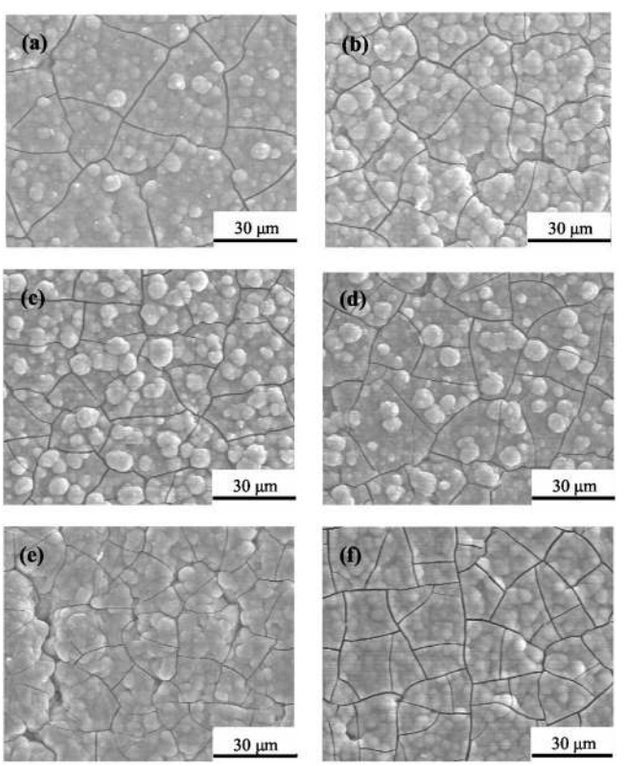

Figure 4. Surface morphologies of the oxides deposited in the 0.25 M manganese acetate solutions with (a) 0, (b) 0.03, (c) 0.05, (d) 0.06, (e) 0.08, and (f) 0.15 M $FeCl_3$ addition.

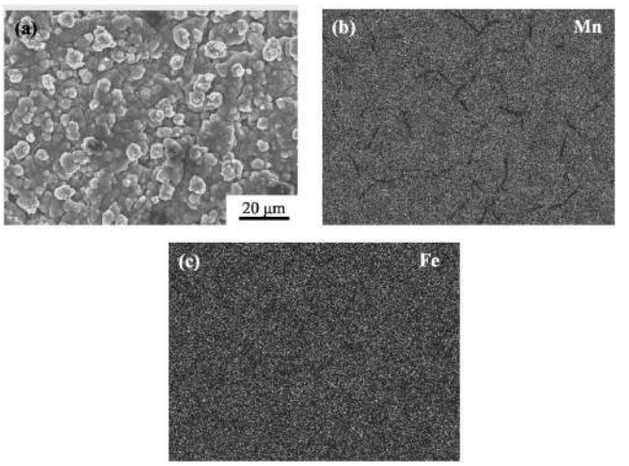

Figure 5. (a) SEM micrograph of the binary Mn/Fe oxide electrode deposited in the plating solution with 0.05 M $FeCl_3$. (b) Mn and (c) Fe EDS mapping results in the area seen in (a).

Mn and Fe elements in the oxide deposited in the plating solution with 0.05 M $FeCl_3$. It was confirmed that both Mn and Fe were uniformly distributed within the oxide. Because similar phenomena were found in the other binary oxides, those data were not shown here. As seen in Fig. 5, the salient and underlying film have the same chemical composition. No segregation can be recognized in this analysis. In order to quantitatively evaluate roughness of the various oxide electrodes, the Ra values were examined by a confocal microscope. The analytical results for the six oxides (demonstrated in Fig. 4) were 682, 752, 920, 850, 680, and 659 nm in sequence. Although the formation mechanism of the oxide morphology still was not very clear, the electrode prepared in the deposition solution with 0.05 M $FeCl_3$ evidently had the roughest surface.

Chemical state.— Because pseudo-capacitance is associated with the faradaic redox reaction of the electroactive material, the chemical states of the deposited oxides are of interest and worthy of being investigated. Figure 6 shows the XPS spectra of Mn $2p_{3/2}$ orbit for various oxides prepared in different deposition solutions. All spectra were quite broad, indicating the oxides may have multi-

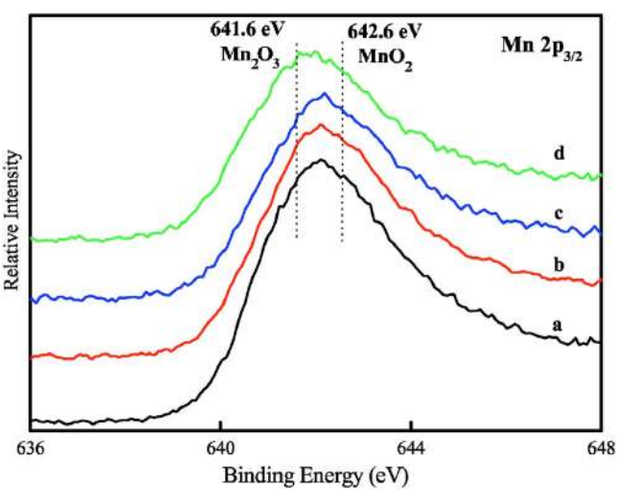

Figure 6. (Color online) XPS spectra of Mn $2p_{3/2}$ orbit for the various oxide electrodes. Curves a–d present the oxides deposited in the 0.25 M manganese acetate solutions with 0, 0.05, 0.10, and 0.15 M $FeCl_3$ addition, respectively.

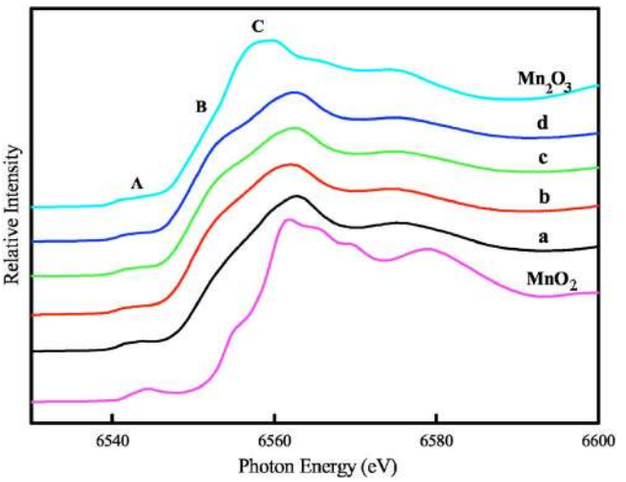

Figure 7. (Color online) Mn K-edge XANES spectra of the various oxide electrodes. Curves a–d present the oxides deposited in the 0.25 M manganese acetate solutions with 0, 0.05, 0.10, and 0.15 M $FeCl_3$ addition, respectively. Analytic results of Mn_2O_3 and MnO_2 standard samples are also included as references.

valence of Mn. It has been reported in the literature[25,26] that the binding energies of Mn $2p_{3/2}$ electron for Mn_2O_3 and MnO_2 were 641.6 and 642.6 eV, respectively. The analytic results, shown in this figure, illustrated that these deposits were composed of both trivalent and tetravalent Mn oxides. Moreover, a chemical shift to lower binding energy was clearly recognized for the oxide deposited in the manganese acetate solution with 0.15 M $FeCl_3$ addition. The data pointed out that the MnO_2/Mn_2O_3 content ratio within the deposited oxide decreased at the high Fe addition condition. X-ray absorption near edge structure (XANES) spectra of the Mn K-edge were measured in order to further explore the variation of Mn chemical state as a function of Fe addition. Obtained spectra of the oxides prepared in various deposition solutions are shown in Fig. 7. Also included are the spectra of two standard references, i.e., Mn_2O_3 and MnO_2 compounds. The results indicated that the curve shapes of the deposited oxides were similar, and the spectra seemed to be contributed by both Mn_2O_3 and MnO_2. A typical XANES spectrum can be divided among a pre-edge range A, a main range B, and a peak area C, followed by the extended X-ray absorption fine structure (EXAFS) oscillations, as marked in Fig. 7. The absorption threshold energy E_0, which can be obtained from the first inflection point in the main absorption range B, was known to be a critical value for determining the valent state of the analyzed element. More specifically, this energy was confirmed to increase with the Mn oxidation state.[27,28] This so-called chemical shift was related to the increase in binding energy of the core-level electron with increasing oxidation state (less valence electrons).[27] According to the spectra shown in Fig. 7, the E_0 of Mn for various oxides can be obtained and are listed in Table I. The results indicated that the valent states of Mn were all between +3 and +4. Moreover, the E_0 was found to gradually decrease with raising Fe addition, revealing the oxidation state of Mn was reduced monotonously. This finding was consistent with XPS analytic results. With increasing $FeCl_3$ in the plating solution up to 0.15 M, the pH value decreased from 7 to around 4. The acidic environment would encourage the electrochemical reduction of tetravalent Mn oxide according to the following equation

$$MnO_2 + H^+ + e^- \rightarrow Mn_2O_3 + H_2O \qquad [2]$$

Accordingly, the above-mentioned variation of Mn oxidation state could be explained.

Figure 8 shows the comparison of Fe $2p_{3/2}$ XPS spectra for the oxides prepared in the manganese acetate solutions with and without $FeCl_3$ addition. Because the spectra of the Fe-added oxides were similar, only a typical datum is demonstrated here. An obvious signal due to Fe addition was detected in curve b of this figure. Moreover, the Fe spectrum can be decomposed into three constituents corresponding to different species such as FeO at 709.7 eV, Fe_2O_3 at 711.0 eV, and FeOOH at 712.1 eV.[29,30] This finding elucidated that both bivalent and trivalent Fe oxides (or hydroxide) coexisted in the oxides deposited in the $Mn(CH_3COO)_2$ and $FeCl_3$ mixed plating solutions. Although Fe^{3+} ions in the plating solution could be incorporated into the oxide simply by the convective flow caused by deposition of Mn oxide near the electrode surface, it was believed that a large part of the Fe^{3+} was reduced to Fe^{2+} before it could be anodically deposited on the substrate. The Fe^{3+} could either receive an electron from Eq. 1 or be reduced by Mn^{2+} in the solution (e.g., $2Fe^{3+} + 2Mn^{2+} + 3H_2O \rightarrow 2Fe^{2+} + Mn_2O_3 + 6H^+$, $E = 0.356$ V, a spontaneous reaction at pH 6, $[Mn^{2+}] = 0.25$ M, $[Fe^{3+}]/[Fe^{2+}] = 1$, and 25°C) and then was transformed to Fe^{2+}. Afterward, two proposed anodic deposition reactions took place, as described below

$$2Fe^{2+} + 3H_2O \rightarrow Fe_2O_3 + 6H^+ + 2e^- \qquad [3]$$

$$Fe^{2+} + 2H_2O \rightarrow FeOOH + 3H^+ + e^- \qquad [4]$$

In addition, the FeO species, which was also detected, could be produced according to the following chemical reaction

$$Fe^{2+} + H_2O \rightarrow FeO + 2H^+ \qquad [5]$$

The variation of Fe valent state with $FeCl_3$ concentration in the deposition solutions can be identified more specifically by X-ray absorption analyses. Figure 9 shows the Fe K-edge XANES spectra of the oxides prepared in various deposition solutions. FeO and

Table I. The threshold energy (E_0), calculated from the Mn K-edge XANES spectra, of various deposited oxides. Analytic results of Mn_2O_3 and MnO_2 standard samples are also included as references.

Sample	Deposition solution	E_0 (eV)
Mn–00Fe	0.25 M $Mn(CH_3COO)_2$	6550.6
Mn–05Fe	0.25 M $Mn(CH_3COO)_2$ + 0.05 M $FeCl_3$	6550.2
Mn–10Fe	0.25 M $Mn(CH_3COO)_2$ + 0.10 M $FeCl_3$	6550.0
Mn–15Fe	0.25 M $Mn(CH_3COO)_2$ + 0.15 M $FeCl_3$	6549.7
MnO_2	—	6552.6
Mn_2O_3	—	6548.2

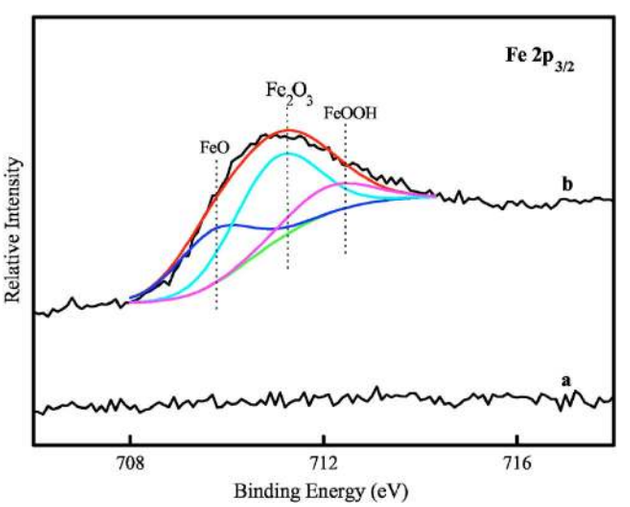

Figure 8. (Color online) XPS spectra of Fe $2p_{3/2}$ orbit for the oxides deposited in the manganese acetate solution without (curve a) and with 0.05 M $FeCl_3$ addition (curve b).

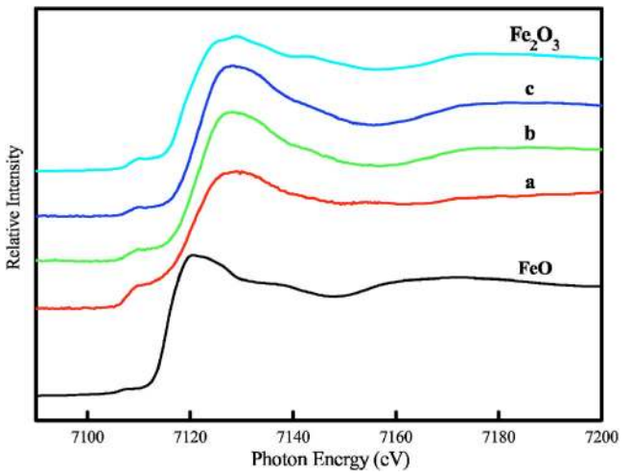

Figure 9. (Color online) Fe K-edge XANES spectra of the various oxide electrodes. Curves a–c present the oxides deposited in the 0.25 M manganese acetate solutions with 0.05, 0.10, and 0.15 M $FeCl_3$ addition, respectively. Analytic results of FeO and Fe_2O_3 standard samples are also included as references.

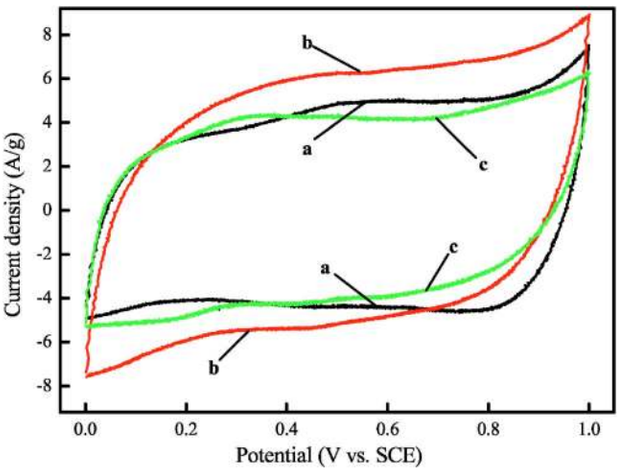

Figure 10. (Color online) Cyclic voltammograms of the various oxide electrodes measured in 2 M KCl electrolyte at a scan rate of 25 mV s^{-1}. Curves a–c present the oxides deposited in the 0.25 M manganese acetate solutions with 0, 0.05, and 0.15 M $FeCl_3$ addition, respectively.

Fe_2O_3 standard samples were also examined and included in this figure as references. Although the spectra of the deposited oxides did not reveal much difference in the shape, the valence of Fe can be recognized by means of finding the E_0 (absorption threshold energy).[28] The E_0 values of the Fe K-edges of the deposited oxides and the two standards (i.e., FeO and Fe_2O_3) were collected and listed in Table II. The data indicated that the oxidation states of Fe were between +2 and +3, which were consistent with the XPS analyses. It was also found that the E_0 increased with the $FeCl_3$ concentration in the deposition solution, revealing the increase in Fe average oxidation state. With high $FeCl_3$ concentration in the solution a low pH environment was established (as described above); accordingly, Eq. 5 was suppressed. Because the amount of the divalent Fe oxide was thus decreased, an increase in the Fe average oxidation state was reasonable. Moreover, considering the monotonous increase in Fe oxidation state (with increasing Fe addition) and the corresponding decrease in the Mn oxidation state, the following interplay reaction between Mn and Fe oxides could not be neglected

$$2MnO_2 + 2FeO \rightarrow Mn_2O_3 + Fe_2O_3 \qquad [6]$$

Electrochemical characteristics.— Electrochemical performance of the oxide electrodes prepared in different deposition solutions were explored by CV. Figure 10 shows the voltammograms of various electrodes, measured in 2 M KCl electrolyte at 25°C, with a potential scan rate of 25 mV s^{-1}. Curve a in this figure was collected from the plain Mn-oxide electrode. Additionally, curves b and c present the oxides deposited in the 0.25 M manganese acetate plating solutions with 0.05 and 0.15 M $FeCl_3$ addition, respectively. All the CV curves were close to rectangular shapes and exhibited mirror-image characteristics. The results demonstrated the excellent reversibility and ideal pseudo-capacitive behavior of the three electrodes. Despite that the curve shapes were similar, Fe addition within the oxides seemed to affect the enclosed area of the CV curves. The larger enclosed area implied that the higher energy density of the oxide could be achieved. According to Fig. 10, the oxide prepared in the deposition solution with 0.05 M $FeCl_3$ had the largest enclosed area (curve b). However, further increasing the $FeCl_3$ concentration up to 0.15 M (curve c) caused the energy-storage capability of the deposited oxide to decrease, even worse than that of the plain Mn oxide (curve a). Specific voltammetric charge (based on weight) of the oxide can be integrated from positive to negative sweeps of the CV curve. Consequently, the specific capacitance (C) of the oxide can be calculated using the following equation

$$C = \text{specific voltammetric charge/potential range} \qquad [7]$$

Specific capacitances of the oxides prepared in various deposition solutions (with different $FeCl_3$ concentrations) were summarized in Table III. The results indicated that the plain Mn oxide had a specific capacitance of 175 F g^{-1}. Capacitance can be improved by a proper amount of Fe addition. As the $FeCl_3$ concentration in the deposition solution was increased to 0.05 M, the specific capacitance of the deposited oxide can reach a maximum of 212 F g^{-1}, which was 21% higher than that of the plain Mn oxide. Nevertheless, the further Fe addition rendered an adverse effect, as recognized in this table. Clearly, the specific capacitance of the oxide decreased monotonously as the concentration of $FeCl_3$ was over 0.05 M. The oxide deposited in the plating solution with 0.15 M $FeCl_3$ only possessed a specific capacitance of 154 F g^{-1}. It is interesting to find a coincidence between the specific capacitance and the oxide surface roughness as a function of Fe addition, as depicted in Fig. 11. The data indicated that the rougher the oxide deposited, the higher specific capacitance can be achieved. Other elements which could affect the electrochemical performance of the oxide electrode included chemical composition and valent state, etc. However, according to this study, surface morphology was considered to be the most important factor that governed the specific capacitance of the binary Mn/Fe oxide.

Electrochemical stability of the oxides prepared in different deposition solutions was evaluated by repeating the CV test for 1000 cycles. The results indicated that the enclosed area of CV curves, for all the electrodes, declined gradually with the cycle number. The active material may have been lost, caused by the dissolution or detachment, and passivated during the charge-discharge cycles in

Table II. The threshold energy (E_0), calculated from the Fe K-edge XANES spectra, of various deposited oxides. Analytic results of FeO and Fe_2O_3 standard samples are also included as references.

Sample	Deposition solution	E_0 (eV)
Mn–05Fe	0.25 M $Mn(CH_3COO)_2$ + 0.05 M$FeCl_3$	7120.2
Mn–10Fe	0.25 M $Mn(CH_3COO)_2$ + 0.10 M$FeCl_3$	7121.3
Mn–15Fe	0.25 M $Mn(CH_3COO)_2$ + 0.15 M$FeCl_3$	7122.4
FeO	—	7119.5
Fe_2O_3	—	7123.2

Table III. Specific capacitances of various deposited oxides at the initial and the 1000th CV cycles. The retained ratios after cycling are also listed.

Sample	Deposition solution	Initial specific capacitance (F g^{-1})	Specific capacitance at 1000th cycles (F g^{-1})	Lost capacitance (F g^{-1})	Capacitance retained ratio (%)
Mn–00Fe	0.25 M $Mn(CH_3COO)_2$	175	123	52	70
Mn–03Fe	0.25 M $Mn(CH_3COO)_2$ + 0.03 $MFeCl_3$	188	156	32	83
Mn–05Fe	0.25 M $Mn(CH_3COO)_2$ + 0.05 $MFeCl_3$	212	180	32	85
Mn–06Fe	0.25 M $Mn(CH_3COO)_2$ + 0.06 $MFeCl_3$	192	161	31	84
Mn–08Fe	0.25 M $Mn(CH_3COO)_2$ + 0.08 $MFeCl_3$	185	157	28	85
Mn–10Fe	0.25 M $Mn(CH_3COO)_2$ + 0.10 $MFeCl_3$	180	153	27	85
Mn–12Fe	0.25 M $Mn(CH_3COO)_2$ + 0.12 $MFeCl_3$	170	143	27	84
Mn–15Fe	0.25 M $Mn(CH_3COO)_2$ + 0.15 $MFeCl_3$	154	131	23	85

the electrolyte. Consequently, degradation of the oxide specific capacitance was recognized. The specific capacitances of the various oxides at the 1000th cycle were shown in Table III. Clearly, the lost capacitances of the deposited oxides during the cycling period decreased with increasing Fe addition (also listed in the table), indicating better electrochemical stability of the oxide with higher Fe content. As compared with the initial capacitance, the capacitance-retained ratio of each oxide electrode can be thus calculated. For the plain Mn oxide, only 70% of the original capacitance was maintained after 1000 CV cycles. However, the capacitance-retained ratios of all the Fe-added Mn oxides were as high as about 85%. Figure 12 shows the surface morphologies of a plain Mn oxide and the binary Mn/Fe oxide deposited in the plating solution with 0.05 M $FeCl_3$ after 200 charge-discharge cycles. Serious dissolution of the plain Mn oxide was clearly observed, while the Fe-added oxide still remained its integrity. To understand which species were dissolved and to evaluate their magnitude quantitatively, these two testing electrolytes were analyzed by AAS. The results indicated that the dissolved Mn concentrations were 0.88 and 0.48 ppm, respectively, for the plain Mn oxide and the binary oxide. No Fe could be detected in the electrolyte. These analytical data confirmed that the corroded species was Mn (or Mn oxide); however, the dissolution can be greatly inhibited by Fe addition. It was believed that the significant improvement in the cyclic stability of the binary oxide electrodes was mainly attributed to the incorporation of the protective Fe oxide.

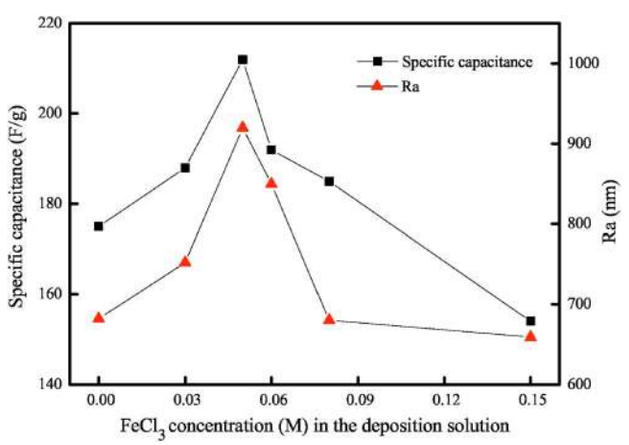

Figure 11. (Color online) Specific capacitance and surface roughness (R_a) of the deposited oxides as a function of $FeCl_3$ concentration (M) in the deposition solution.

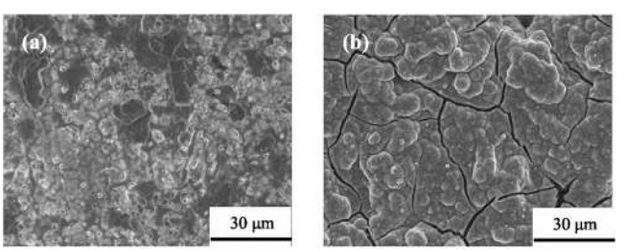

Figure 12. Surface morphologies of the (a) plain manganese oxide and (b) Fe-doped manganese oxide after 200 charge-discharge cycles. The latter one was deposited in the 0.25 M manganese acetate solution with 0.05 M $FeCl_3$ addition.

Conclusion

First, the Fe-added Mn oxide was successfully prepared on the graphite substrate by anodic deposition. Fe/Mn content ratio within the oxide can be controlled by adjusting the $FeCl_3$ concentration in the 0.25 M $Mn(CH_3COO)_2$ aqueous deposition solution. Second, the incorporated Fe existed as FeO, Fe_2O_3, and FeOOH forms in the oxide according to XPS analysis. However, the Fe addition did not change the nanocrystalline structure of the deposited Mn oxides. Third, surface morphology (or roughness) of the oxide electrode strongly depended on the amount of Fe addition. The oxide deposited in the plating solution with 0.05 M $FeCl_3$ possessed the roughest surface. Fourth, the material modifications of the oxide electrode, caused by Fe addition, could lead to an evident improvement of its pseudo-capacitive performance. Optimum specific capacitance of the Mn/Fe oxide, which showed the greatest surface roughness, was 212 F g^{-1}. The value was 21% higher than that of the plain Mn oxide. Moreover, capacitance-retained ratio of the oxide electrode after 1000 charge-discharge cycles was also improved from 70 to 85% due to Fe addition.

Acknowledgments

The authors would like to thank the National Science Council of China for financially supporting this research under contract no. NSC 93-2216-E-006-044.

National Cheng Kung University assisted in meeting the publication costs of this article.

References

1. R. Kötz and M. Carlen, *Electrochim. Acta*, **45**, 2483 (2000).
2. B. E. Conway, *J. Electrochem. Soc.*, **138**, 1539 (1991).
3. J. P. Zheng, J. Huang, and T. R. Jow, *J. Electrochem. Soc.*, **144**, 2026 (1997).
4. M. Ishikawa, M. Morita, M. Ihara, and Y. Matsuda, *J. Electrochem. Soc.*, **141**, 1730 (1994).
5. B. Pillary and J. Newman, *J. Electrochem. Soc.*, **143**, 1806 (1996).
6. S. Sarangapani, B. V. Tilak, and C. P. Chen, *J. Electrochem. Soc.*, **143**, 3791 (1996).
7. C. C. Hu and Y. H. Huang, *J. Electrochem. Soc.*, **146**, 2465 (1999).
8. K. C. Liu and M. A. Anderson, *J. Electrochem. Soc.*, **143**, 124 (1996).
9. Y. Takasu, S. Mizutani, M. Kumagai, S. Sawaguchi, and Y. Murakami, *Electrochem. Solid-State Lett.*, **2**, 1 (1999).
10. H. Y. Lee and J. B. Goodenough, *J. Solid State Chem.*, **144**, 220 (1999).
11. H. Y. Lee and J. B. Goodenough, *J. Solid State Chem.*, **148**, 84 (1999).
12. C. Z. Deng, R. A. J. Pynenburg, and K. C. Tsai, *J. Electrochem. Soc.*, **145**, L61 (1998).
13. T. C. Liu, W. G. Pell, B. E. Conway, and S. L. Roberson, *J. Electrochem. Soc.*, **145**, 1882 (1998).

14. A. Laforgue, P. Simon, C. Sarrazin, and J. F. Fauvarque, *J. Power Sources*, **80**, 142 (1999).
15. S. C. Pang, M. A. Anderson, and T. W. Chapman, *J. Electrochem. Soc.*, **147**, 444 (2000).
16. S. C. Pang and M. A. Anderson, *J. Mater. Res.*, **15**, 2096 (2000).
17. C. C. Hu and T. W. Tsou, *Electrochem. Commun.*, **4**, 105 (2002).
18. J. K. Chang and W. T. Tsai, *J. Electrochem. Soc.*, **150**, A1333 (2003).
19. J. K. Chang and W. T. Tsai, *J. Appl. Electrochem.*, **34**, 953 (2004).
20. J. K. Chang, C. T. Lin, and W. T. Tsai, *Electrochem. Commun.*, **6**, 666 (2004).
21. N. L. Wu, S. Y. Wang, C. Y. Han, D. S. Wu, and L. R. Shiue, *J. Power Sources*, **113**, 173 (2003).
22. T. Brousse and D. Bėlanger, *Electrochem. Solid-State Lett.*, **6**, A244 (2003).
23. S. Y. Wang, K. C. Ho, S. L. Kuo, and N. L. Wu, *J. Electrochem. Soc.*, **153**, A75 (2006).
24. S. Y. Shiue and N. L. Wu, *J. Appl. Electrochem.*, **33**, 345 (2003).
25. B. R. Strohmeier and D. M. Hercules, *J. Phys. Chem.*, **88**, 4922 (1984).
26. B. N. Ivanov-Emin, N. A. Nevskaya, B. E. Zaitsev, and T. M. Ivanova, *Zh. Neorg. Khim.*, **27**, 3101 (1982).
27. P. Ghigna, G. Flor, and G. Spinolo, *J. Solid State Chem.*, **149**, 252 (2000).
28. S. Quartieri, M. P. Riccardi, B. Messiga, and F. Boscherini, *J. Non-Cryst. Solids*, **351**, 3013 (2005).
29. N. S. McIntyre and D. G. Zetaruk, *Anal. Chem.*, **49**, 1521 (1977).
30. T. C. Lin, G. Seshadri, and J. A. Kelber, *Appl. Surf. Sci.*, **119**, 83 (1997).